ARCHIVES OF TRANSPORT *ISSN (print):* *0866-9546*
Volume 71, Issue 3, 2024 ***e-ISSN (online):*** *2300-8830*
DOI: *10.61089/aot2024.fspnvx83*

WHEEL-RAIL WEAR CHARACTERISTICS OF A MODERN TRAM PASSING CURVES WITH SMALL RADIUS

Zhongjie ZHANG[1], Xinwen YANG[2], Yanyan ZHANG[3], Caixia MIAO[4], Yipeng CUI[5], Jiqiang SHEN[6]

[1, 4, 5, 6] *Rail Transit and Underground Space Research Institute, Shanghai Urban Construction Design and Research Institute (Group) Co., Ltd, Shanghai, China*
[2, 3] *Shanghai Key Laboratory of Rail Infrastructure Durability and System Safety, Tongji University, Shanghai, China*

Abstract:

The wheel-rail wear was predicted for modern trams with independently rotating wheelset running on a groove-shaped rail. The tram vehicle-track coupled dynamics model, considering the wheel-rail multi-point contact, was developed using software UM to evaluate the dynamic responses of the vehicle and track. Hertz contact theory, the FastSim algorithm, and Archard material wear model were used to solve the normal contact stress, tangential contact stress, and wheel-ail wear, respectively. The wheel and rail profiles were updated when the wear depth reached to 0.1 mm. In calculation, the wheel and rail wear was calculated and analyzed separately. The results of groove rail and independently rotating wheelset wear predicted by this model coincided with relevant literature, which proved the effectiveness of this model. The wheel and rail wear characteristics of modern trams passing through curved tracks with small radii and the influence of wheel-rail friction coefficient on wheel and rail wear were calculated and analyzed using this model. The results show that the wheel and rail wear on the circular curve and the rear transition curve is more intense. The wheel wear is the most intense on circular curve while the rail wear is on the rear transition curve. The wear of inner and outer rails and wheels of wheelset one increases with the increase of wheel-rail friction coefficient while the wear of inner and outer wheels of wheelset three have no obvious change. The wear of the inner and outer rails is the most intense at the gauge corner position while is the lightest at the guard rail. The wear of wheelset one is more intense than that of wheelset three and the inner wheel wear is more intense than that of the outer wheel. The present analysis contributes to improve the life of tram wheel and rail and reduce the frequency of wheel-rail maintenance during operation.

Keywords: *modern trams, groove-shaped rail, independently rotating wheels, curved track, wheel-rail wear, characteristics*

To cite this article:

Zhang, Z., Yang, X., Zhang, Y., Miao, C., Cui, Y., Shen, J., (2024). Wheel-rail wear characteristics of a modern tram passing curves with small radius. Archives of Transport, 71(3), 67-90. DOI: https://doi.org/10.61089/aot2024.fspnvx83

Contact:
1) zhangzhongjie@sucdri.com [https://orcid.org/0009-0008-9766-268X]; 2) xinwenyang@tongji.edu.cn [https://orcid.org/0000-0001-8209-1257] – corresponding author; 3) yanyan2030@126.com [https://orcid.org/0000-0002-5896-4123]; 4) miaocaixia@sucdri.com [https://orcid.org/0009-0007-2566-5649]; 5) cuiyipeng@sucdri.com [https://orcid.org/0009-0002-4139-5021]; 6) shenjiqiang@sucdri.com [https://orcid.org/0009-0003-2169-0450]

1. Introduction

Modern trams are employed by more and more cities because of their energy saving, environmental protection and low cost. In recent years, modern tram projects in China have shown a large-scale and high-speed development trend. Modern trams mostly adopt low-floor structure, which leads to the extensive use of independently rotating wheels. Modern tram lines have the characteristics of large number of small curves, intense and complicated wheel-rail interaction (Zeng et al., 2021). The running principle of independently rotating wheelset bogies is completely different from that of traditional wheelset bogies. In theory, there is no reset torque in the independently rotating wheelset and so the self-centering ability on straight line and self-steering ability during curve negotiation of the traditional rigid wheelset bogies no longer exist in the independently rotating wheelset bogies (Suda et al., 2023). During curve passing, the attack angle and the wheel-rail lateral force of the independent rotating wheelset is large while on tangent track, the wheel flange is close to the rail, resulting in large wheel flange wear and high derailment risk (Chi et al., 2008).

Model-driven method and data-driven method are two main traditional wheel-rail wear predict methods in the last decades. The model-driven method predicts the wear with the developed vehicle-rail coupled physical model and is not dependent on large amounts of historical tracking wear data (Zhu et al., 2019). The core content of this method is to solve the wheel-rail rolling contact problem, and to numerically simulate and predict the wheel-rail contact wear by combining the vehicle-rail coupling dynamics model and material wear model. Archard model is the most commonly used material wear model (Pradhan et al., 2019). Before employing material wear model, it is necessary to develop the physical models of vehicle and track to obtain the vehicle dynamics characteristics and wheel-rail contact characteristics. At present, there are some commercial software such as UM (Wang et al., 2022a), SIMPACK (Li et al., 2020) and MATLAB (Chudzikiewicz et al., 2018) have the wheel-rail wear simulation module. This module has already integrated the models of vehicle dynamics, wheel-rail contact, and material wear models and is convenient for people to use according to their actual demands.

Data-driven methods try to obtain the hidden information from the historical tracking wear data without detailed and complex physical process, and then predict the features from the given data. Probability statistical model and machine learning method are two types of data-driven methods received attention from scholars. The statistical model devotes itself to establish a linear and nonlinear correlation between wear data and time (Wang et al., 2015; Zeng et al., 2020). When the amount of data is large, machine learning with automatic learning and decision-making abilities often has excellent prediction performance and has been the first choice. The most well-known machine learning for wheel-rail wear prediction is the artificial neural network technology, such as wavelet neural network (Wang et al., 2022b), feedforward neural network (Shebani et al., 2018), and backpropagation neural network (Wang et al., 2018). Note that the basic parameters of a neural network always need to be optimized by some non-numerical optimization algorithms such as particle swarm optimization algorithm (Cai et al., 2022) and genetic algorithm (Su et al., 2023).

The grooved rail widely used in modern tram line is helpful to the small radius curve operation due to the existence of the guard rail, but it also causes the wear between the wheel back and the guard rail. So, the wheel-rail wear of tram has its own characteristics. A series of tests have been carried out on the problem of tram wheel-rail wear (Zhao et al., 2011; Liu et al., 2024). During the measurement, it is found that the tread of some inner and outer rails deviated from the original profiles and the regular wave wear was the main one on small curved track whose radius was below 400 m. In Łuczak et al. (2020), The 60R2 groove rail was taken as an example to predict the tram wheel wear in complex motions. Wheel-rail profile optimization is an effective method to control wheel-rail wear. A wheel tread profile design method was proposed based on the contact angle difference, and a corresponding computer-aided design program was developed (Zhong et al., 2016). A grooved rail profile optimization model was established based on augmented Gaussian radial primary function (AGRPF), and the model was solved by sequential quadratic programming (SQP) and multi-objective optimization principle (Yang et al., 2022). Compared with the original tread, the optimized one increased the restore ability of the independently rotating wheelset and improved the wheel/rail contact

state and reduced the wheel/rail contact stress. To track and identify the early signs of wear, Wojciechowski et al. (2020) focused on mechanism identification and wheel surface topography to analyze the tram wheel wear characteristics. Out-of-round railway wheels continuously excites the vehicle-track system. So, Zehetbauer et al. (2024) researched the wheel polygonal wear evolution on a two axle tram bogie. It has been found that wheel-rail contact conditions and related creepage-creep force characteristics appear to be decisive for the evolution directions and evolution speeds.

When the tram passing through a curved track with small radius, the problems of uneven wheel-rail wear are highlighted. The more intense problem is that the strong wheel-rail interaction also causes excessive vibration and noise radiation and intensely affects the ride comfort of passengers. In order to explore the modern trams wheel-rail wear characteristics when passing through a small radius curve, a wheel-rail wear prediction model is established based on model-driven method in this paper. The tram vehicle-track coupled dynamics model considering wheel-rail multi-point contact is developed using UM. Hertz contact theory, the FastSim algorithm, and Archard material wear model are used to solve the normal contact stress, tangential contact stress, and wheel-rail wear, respectively. Based on this model, the wheel-rail wear characteristics of modern trams passing through a small radius curved track are calculated and analyzed.

2. Methodology

2.1. Architecture of wheel-rail wear prediction model

The architecture of the wheel-rail wear prediction model of tram is shown in Figure 1. This model consists of four modules: (1) A multi-rigid-body multi-degree-of-freedom vehicle-track coupled dynamics model constructed in software UM used to evaluate the dynamic responses of the vehicle and track; (2) The wheel–rail contact modelled by Hertzian theory and FastSim algorithm respectively to calculate the normal and tangential forces; (3) A wear model established by Archard theory for wear calculation; (4) wheel-rail profile updating strategy. The calculation process of the wheel-rail profile prediction model is as follows:

Step 1: The dynamic parameters of the wheel-rail contact point are solved by using the tram vehicle-track coupled dynamics model.

Step 2: The normal contact stress is solved by Hertz contact theory, and then the tangential contact stress is solved by the simplified method of the rolling contact.

Step 3: The wheel-rail wear is calculated based on the Archard material wear model.

Step 4: After the wear depth reaches to 0.1 mm, the wheel and rail profiles are updated and the next iteration starts.

In addition, the single variable method is used to calculate and analyze the wheel and rail wear, that is, the wheel and rail wear is calculated and analyzed separately.

2.2. Modern tram vehicle-track coupled dynamics model

The modern tram line is generally laid with groove rail. In this paper, 60R2 rail is selected, and its cross-section shape is shown in Figure 2. Among them, A, B and C represent the top surface of rail, gauge corner and guard rail position respectively. The width of area A is 55.8mm, which is composed of 5 arcs (with the numbers ① — ⑤) with radii of (5, 80, 300, 80, 13) mm.

The multi-body dynamics simulation software Universal Mechanism (UM) is used to model the modern tram vehicle-track coupled dynamics model. The vehicle is organized in the form of “motor car + trailer car + motor car”, as shown in Figure 3. The wheel tread profile is shown in Figure 4. In a motor vehicle, secondary suspensions couple the bogie frame to the carbody through a bolster and primary suspensions support the bogie frame on two rigid wheelsets. In the trailer vehicle, the bogie frame is directly coupled with the carbody and two independently rotating wheelsets through primary suspensions. The left and right independently rotating wheels are connected to a crankshaft by revolute joints. The primary and secondary suspension systems are regarded as spring-damping units. During constructing the vehicle-track coupled dynamics model, some main assumptions are made as follows: (1) The rail and the components of wheelset, bogie frame and carbody are regarded as rigid bodies, ignoring their elastic deformation; (2) the structure of the wheelset, bogie frame and carbody is completely

symmetrical. The basic parameters of the vehicle are shown in Table 1.

2.3. Wheel-rail wear calculation model

The calculation formula of wheel-rail material wear is based on Archard material wear algorithm (Yang et al., 2019).

$$V_w = K_A \frac{ND}{H} \tag{1}$$

where, V_w is the wear volume; K_A is the wear factor; N is the normal contact force; D is the sliding distance between wheel and rail, which is related to the relative sliding speed of wheel and rail and the longitudinal, lateral and spin creep rates of wheel and rail; H is the hardness of the softest contacting surfaces. The formula for calculating the sliding distance D is as follows:

$$D = \left|v_{\text{slip}}\right| \frac{\triangle x}{v_0} \tag{2}$$

where, v_{slip} is the relative sliding speed of wheel and rail; Δx is the length of a rectangular element in the longitudinal direction of the rail; v_0 is the wheel rolling speed.

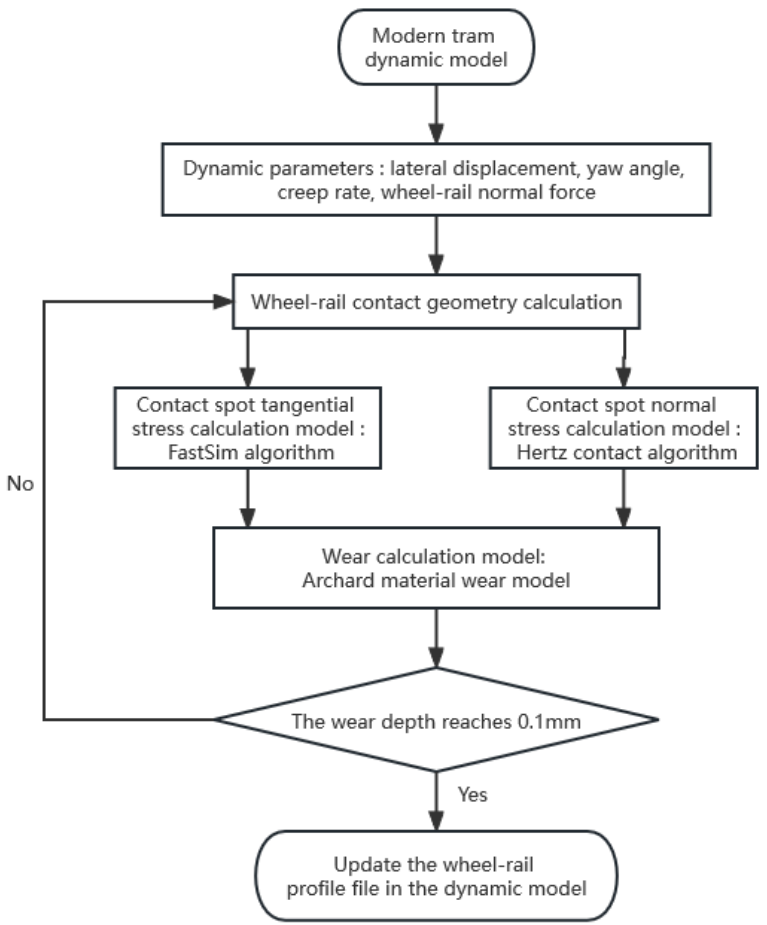

Fig. 1. Flow chart of wheel-rail wear prediction

The wear factor depends on the wheel-rail contact pressure and the relative sliding velocity on the contact point, as shown in Fig. 5. The horizontal axis represents the sliding velocity, and the vertical axis represents the wheel-rail contact pressure. Region I indicates that the sliding velocity and contact pressure are both small, which means that the wheel-rail contact wear is small. Region II indicates that the sliding velocity is between 0.2m/s and 0.7m/s and the wear is more intense. In region III, the sliding velocity is larger than 0.7m/s. Regions I ~III is a slight wear stage with small contact pressure. When the contact pressure is greater than 0.8H, it is the stage of destructive wear (region IV).

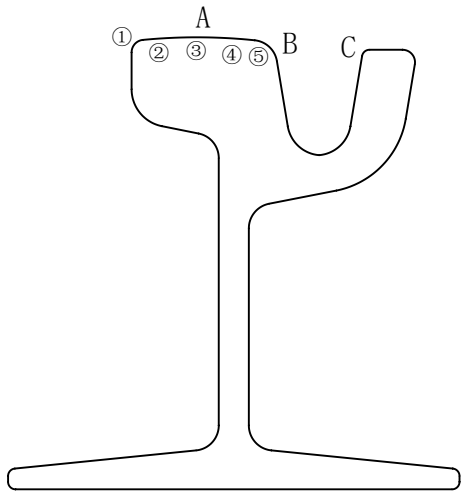

Fig. 2. Cross-section of groove rail

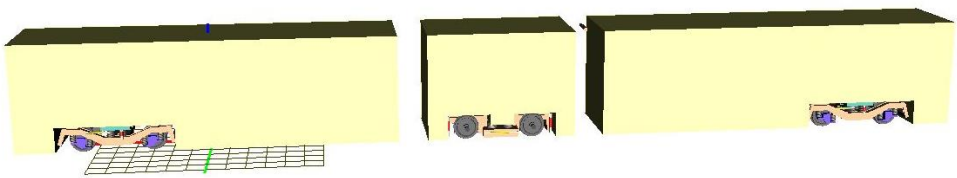

(a) Modern tram

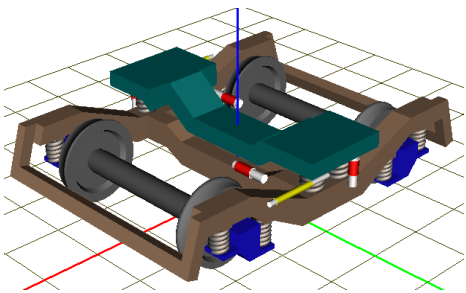

(b) Motor bogie

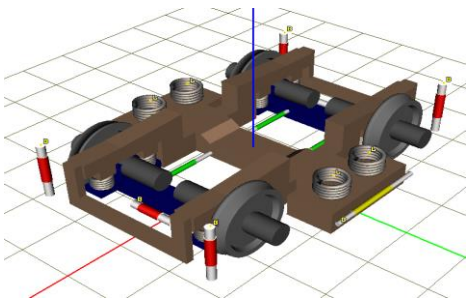

(c) Trailer bogie

Fig.3. Dynamics model of modern tram

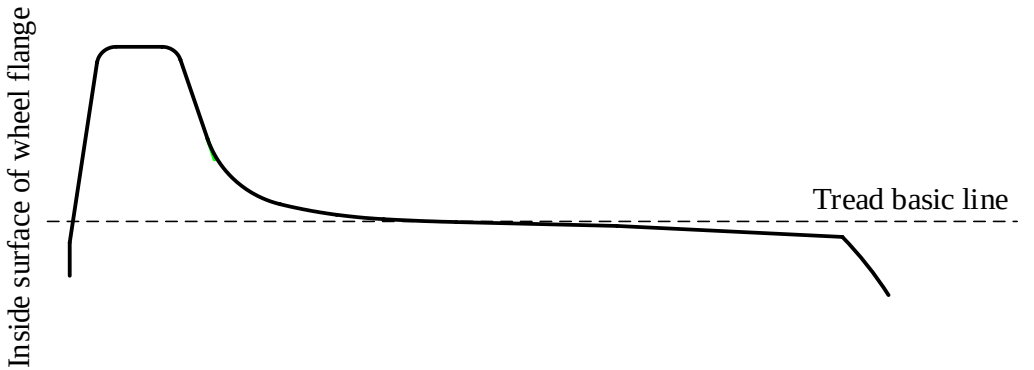

Fig. 4. Tread profile

Table. 1. Basic parameters of the vehicle.

Parameters	Value
Maximum running speed (km/h)	70
Axle load (t)	12
Wheel diameter (mm)	660
Wheelbase (mm)	1800
Minimum curve radius (m)	25
Distance between bogie centers (m)	10.4
Vehicle body height (m)	3.6
Vehicle body width (m)	2.65

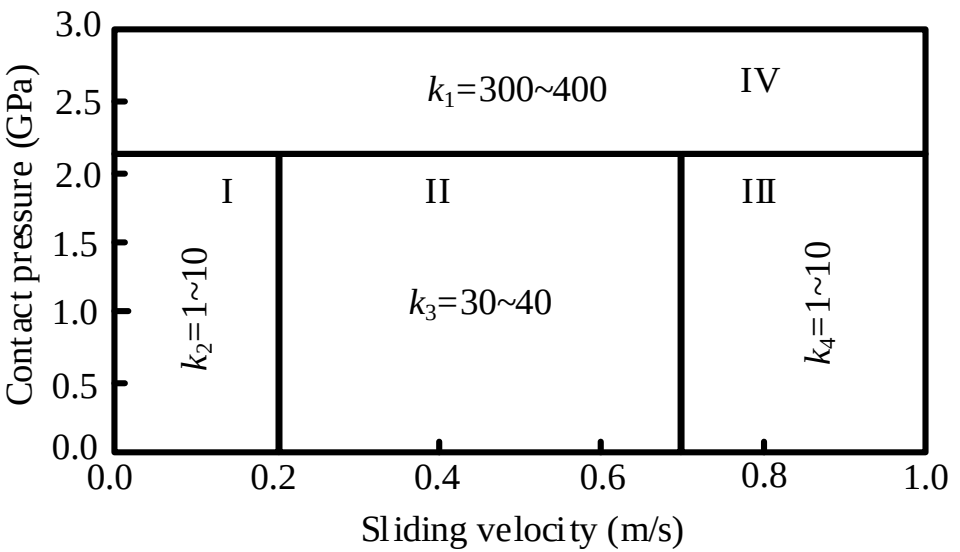

Fig. 5. Wear factor distribute on

the contact patch is divided into several rectangular elements, and the wear depth at the center of any rectangular element in the contact patch is:

$$\Delta z = \frac{\Delta V_w}{\Delta A} = K_A \cdot \frac{p\ (x,y)\ \Delta d}{H} \tag{3}$$

where, ΔA is the area of the rectangular element; $p(x, y)$ is the wheel-rail normal stress distribution; Δd is the sliding amount of any rectangular element.

In this paper, a simplified rail wear calculation method is adopted: When the wheel rolls over the contact patch, the calculation results on the wheel-rail contact patch do not change. Therefore, the total wear of rail contact point can be obtained by superimposing the wear of each rectangular element in the same longitudinal direction within the same contact patch (Eq. (4)).

$$\Delta z = \sum_{x=1}^{n} \Delta z_y(x,y) \quad (y = 1 \sim n) \tag{4}$$

where Δz is the total wear in the same longitudinal direction; Δz_y is the wear of each rectangular element in the longitudinal direction; n is the rectangular element number.

After calculating the wear of each wheel passing through a contact patch, the wear of each wheel is superimposed to get the total wheel wear.

The average wear rate can be expressed as follows:

$$p = \frac{\sum p_i}{n-1} \tag{5}$$

$$p_i = \frac{|z_{i+1} - z_i|}{z_i} \quad i = 1,2,\ldots,n-1 \tag{6}$$

where n is the number of influence factor; z_i is the i-th wear.

3. Numerical analysis and discussion

3.1. Model validation

In order to verify the correctness of the wheel-rail profile prediction model of modern trams in this paper, the same calculation conditions and parameters as in (Ding et al., 2017) are selected. The models in this paper and in (Ding et al., 2017) have identical components and the assumptions in these models are the same. The outside rail wear calculation results of the prediction model in this paper are compared with the results of the model in (Ding et al., 2017), as shown in Figure 6. Taking the independently rotating wheelset of the trailer as an example, the calculation results of the wheel wear after 30 iterations are shown in Figure 7.

It can be seen from Figure 6 and Figure 7 that the calculation results in this paper are in the same order of magnitude as those in (Ding et al., 2017). The wheel-rail wear position and variation law reflected by the data are generally similar, and the wear value is not much different. After the train passes more than 15, 000 times, the relative error of the wear depth of outside groove rail is 7.18%, of outer wheel wear is 1.33%, and of inner wheel wear is 31.41%. Therefore, it can be concluded that the model in this paper can be used for the prediction and subsequent analysis of wheel-rail wear of modern trams.

3.2. Wheel-rail wear characteristics

The line conditions for calculation and analysis are selected as shown in Figure 8. Point A is the midpoint of the front transition curve; point B is the midpoint of the circular curve; point C is the midpoint of the rear transition curve; V is the speed; R is the radius of curved track; h is the super-elevation for the outer rail.

Figure 9 is the profile change diagram of the inner and outer rails of each section of the line after the tram passes 100, 000 times, and Figure 10 is the wear diagram of the inner and outer rails of each section of the line after the tram passed 100, 000 times. It can be seen from Figure 9 and Figure 10 that on the line with a curve radius of 50 m, after the tram passed 100, 000 times, the rail wear of the circular curve and the rear transition curve is much larger than that of the front transition curve, and the wear of the rear transition curve is the most intense. The total rail wear of the rear transition curve is 119% of the total wear of the circular curve and 344% of the total wear of the front transition curve.

Figure 11 is the wheel wear of the inner and outer wheels of wheelsets one and three after the tram passed 1 000 km. The wheelset one is a traditional integrated wheelset, and the wheelset three is an independently rotating wheelset.

It can be seen from Figure 11 that on the line with a curve radius of 50 m, after the tram passed through 1 000 km, the wheel wear on the circular curve and the rear transition curve is more intense than that on

the front transition curve. The total wheel wear of the circular curve is 120% of the total wear of the rear transition curve and 308% of the total wear of the front transition curve.

By comparing the wear of wheelset one and wheelset three in Figure 11, it can be seen that the wear of wheelset one, that is, the traditional rigid wheelset, is more intense than that of wheelset three, that is, the independently rotating wheelset. The wear of wheelset one is concentrated in the gauge corner position, and the wear of the wheelset three is concentrated in the rail head position.

(a) Calculation results of this paper

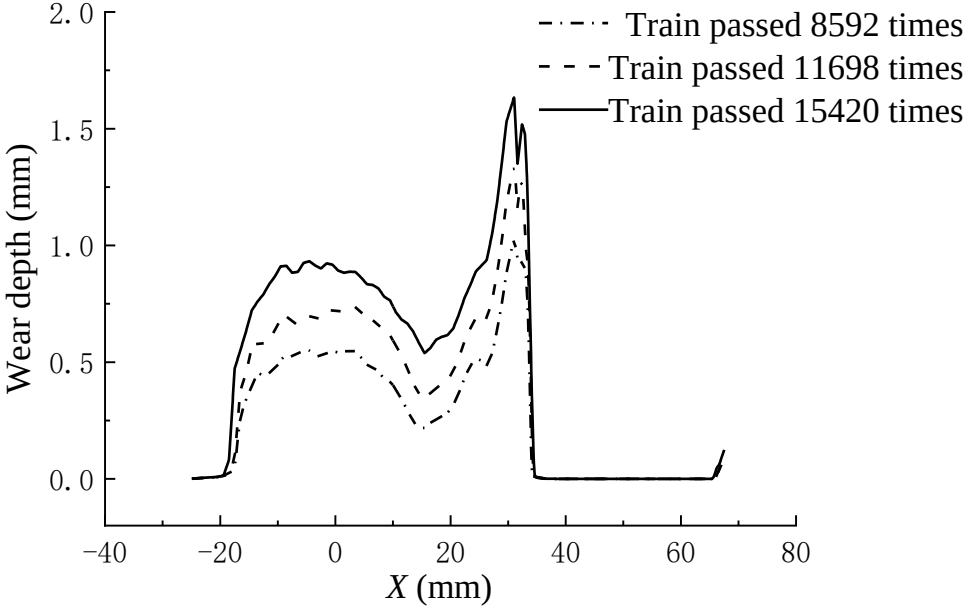

(b) Calculation results in (Ding et al., 2017)

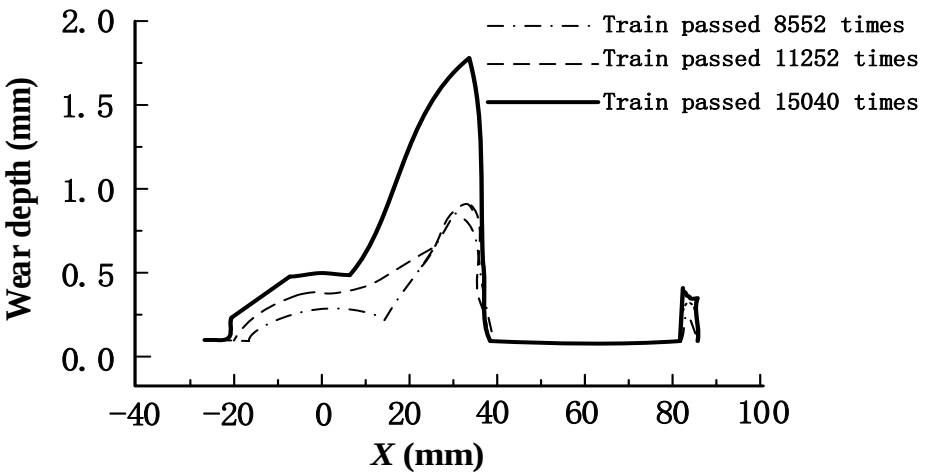

Fig. 6. Comparison of wear of outside groove rail.

(a) Outer wheel wear

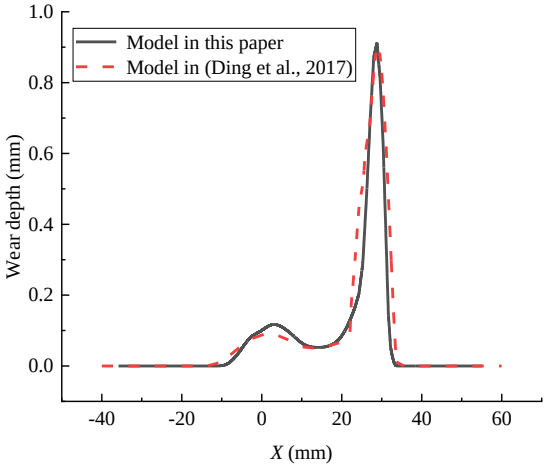

(b) Inner wheel wear

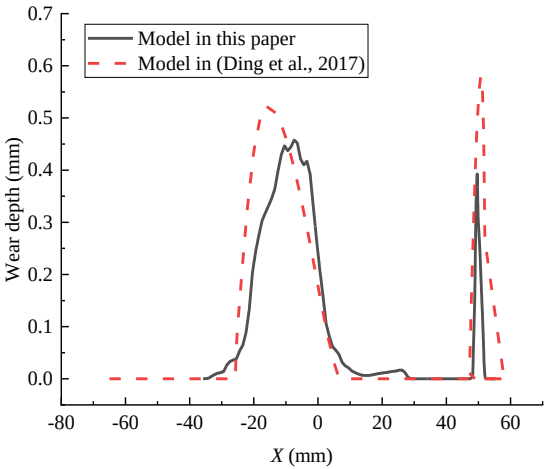

Fig. 7. Comparison of wear of modern tram's independently rotating wheelset

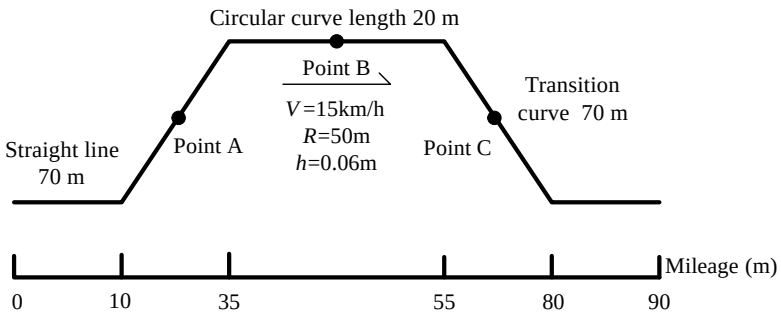

Fig.8. Parameters of curved track

(a) Variation of inner rail profile

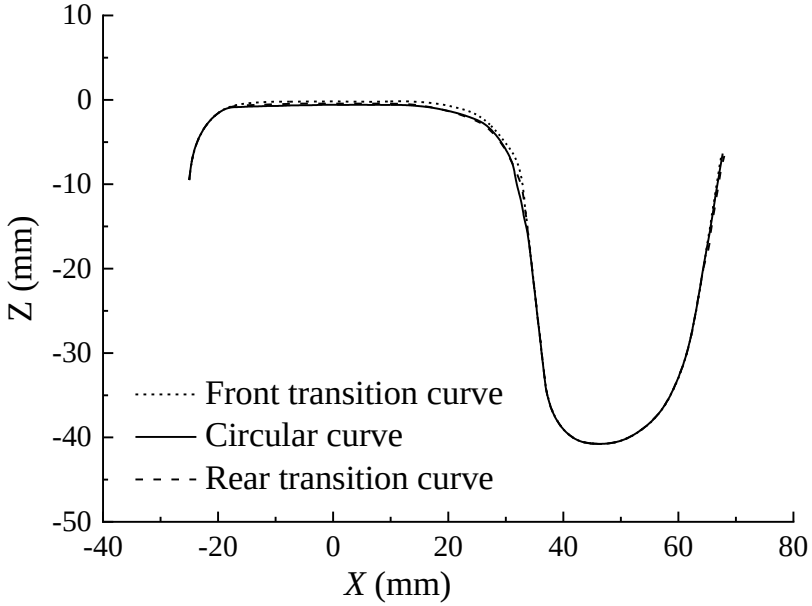

(b) Enlarged diagram of inner rail profile change

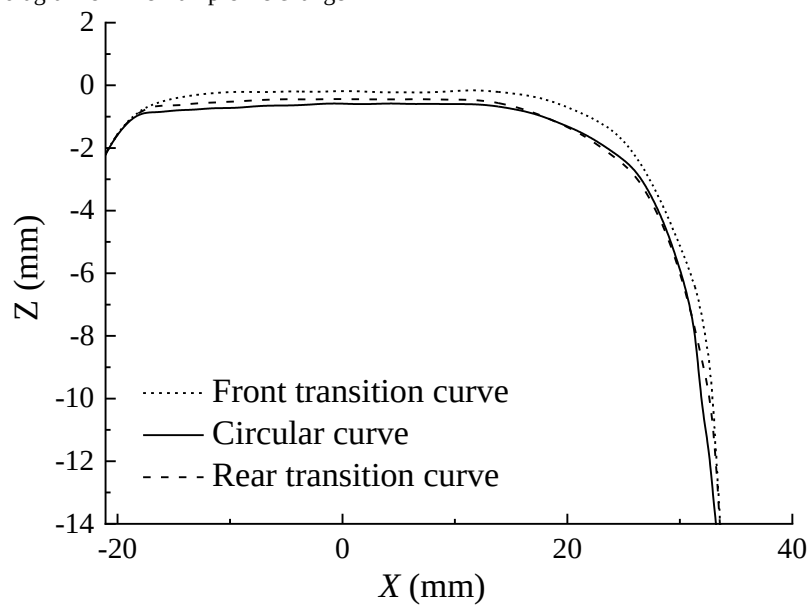

Fig. 9. (a)-(b). Changes in the inner and outer rail profiles at different positions on the curve after tram passed 100, 000 times.

(c) Change of outer rail profile

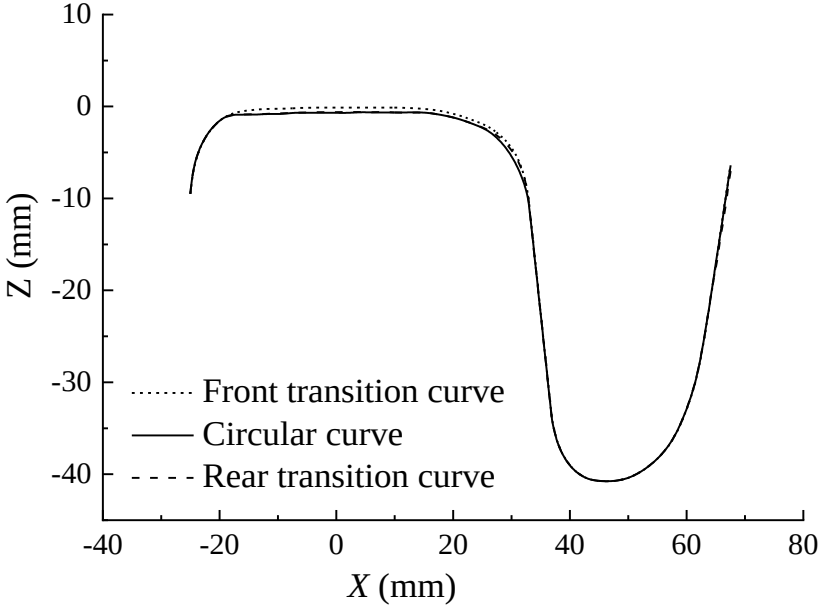

(d) Enlarged diagram of outer rail profile change

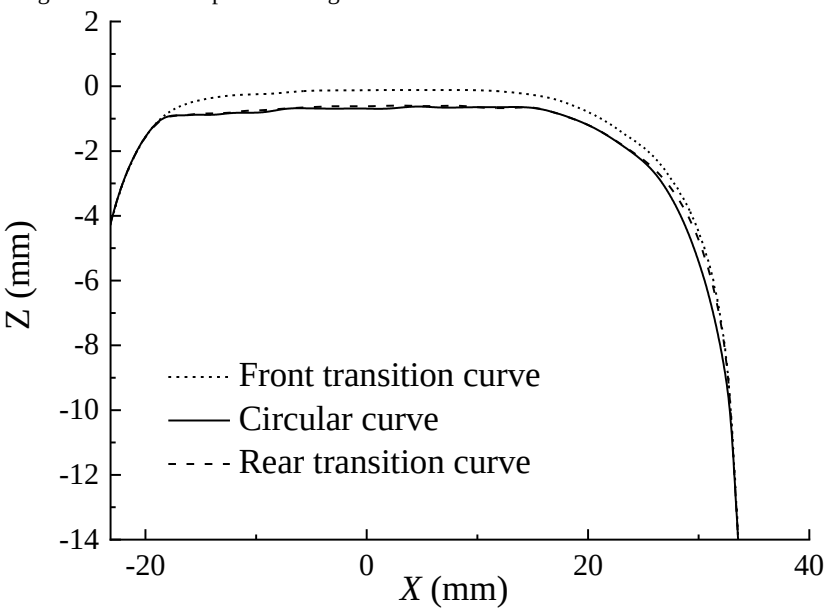

Fig. 9.(c)-(d) Changes in the inner and outer rail profiles at different positions on the curve after tram passed 100, 000 times

(a) Inner rail wear diagram

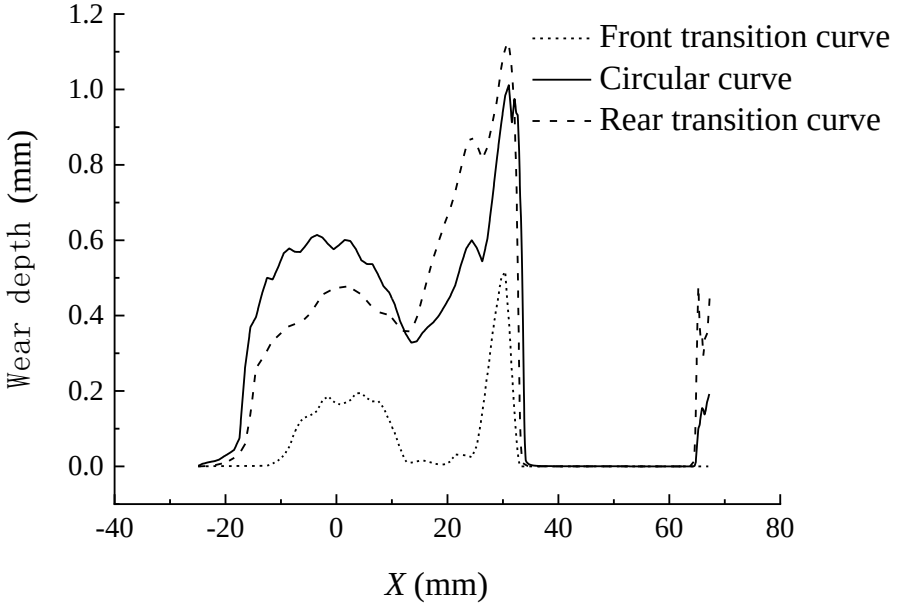

(b) Outer rail wear diagram

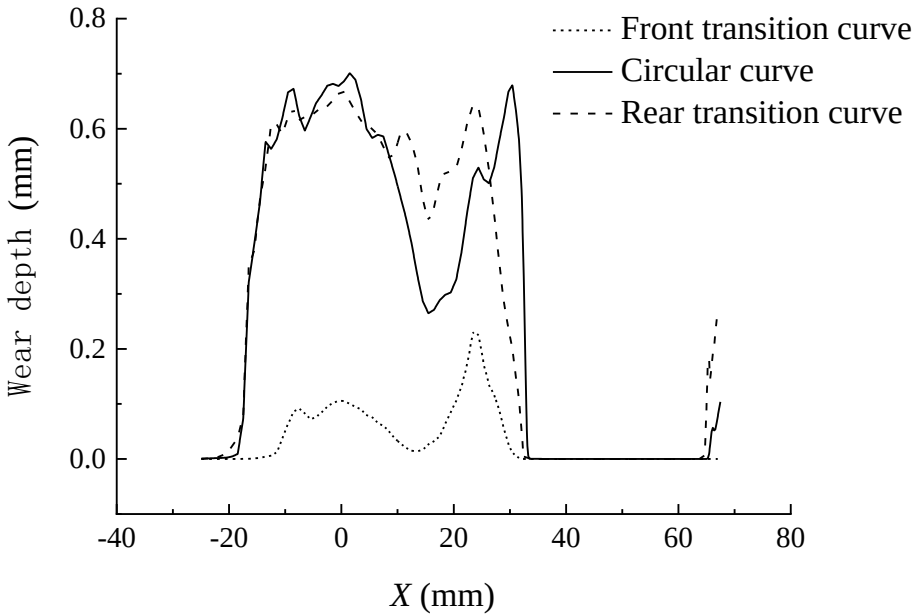

Fig. 10. Diagram of inner and outer rail wear after tram passed 100, 000 times.

(a) Inner wheel of wheelset one

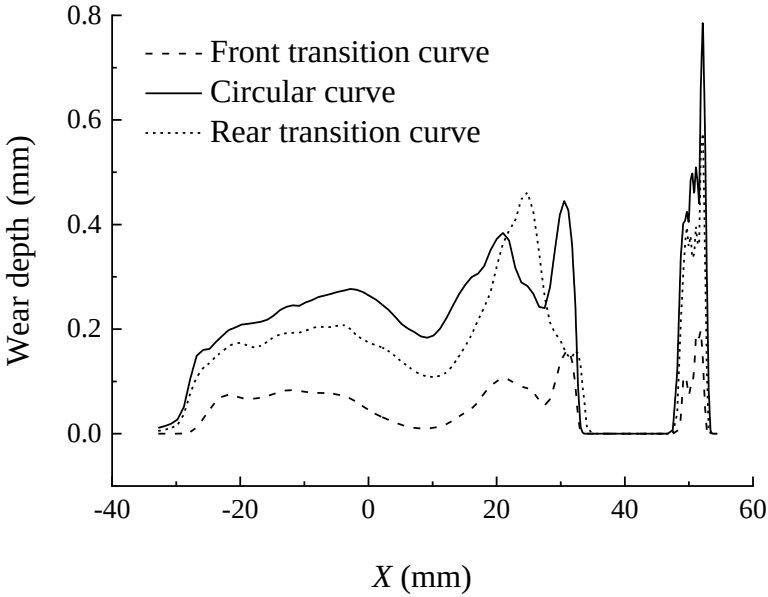

(b) Outer wheel of wheelset one

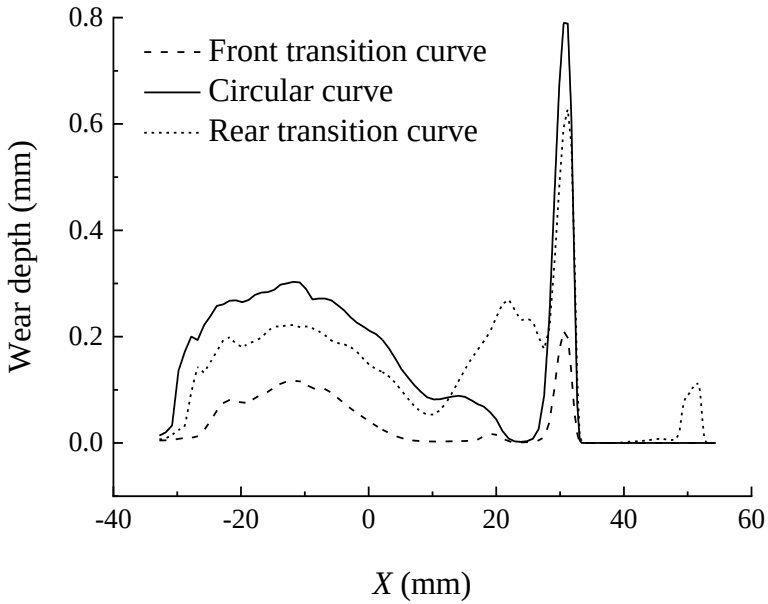

Fig. 11.(a)-(b) Wheel wear of the inner and outer wheels at different positions on the curve after tram passed through 1 000 km

(c) Inner wheel of wheelset three

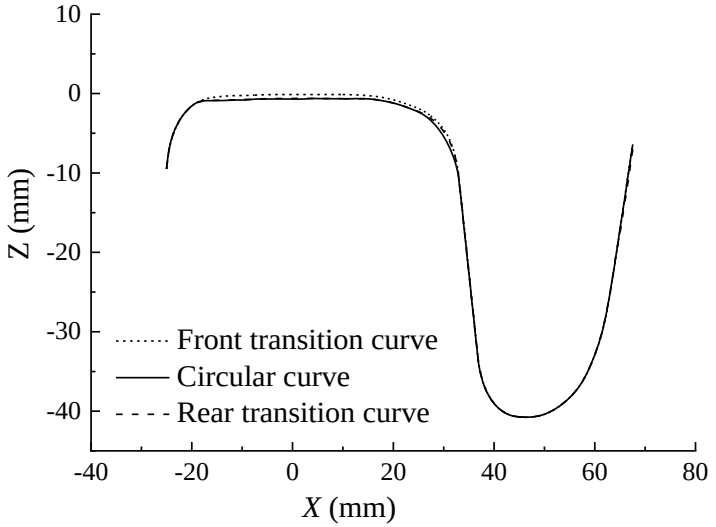

(d) Outer wheel of wheelset three

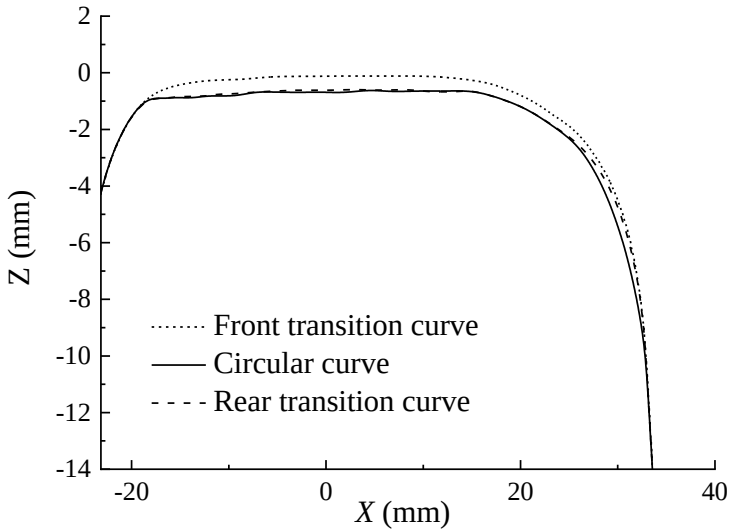

Fig. 11.(c)-(d) Wheel wear of the inner and outer wheels at different positions on the curve after tram passed through 1 000 km

3.3. Influence of wheel-rail friction coefficient

Figure 12 is the profile change diagram of the inner and outer rails after the tram passed 68 000 times under three wheel-rail friction coefficients: 0.2, 0.3 and 0.4. Figure 13 is the wear of the inner and outer rails after the tram passed 68 000 times under those friction coefficients. Table 2 is the maximum rail wear after 68 000 times tram passed under three friction coefficients.

It can be seen from Figure 12, Figure 13 and Table 2 that the wear of inner and outer rail increases with the increase of wheel-rail friction coefficient. The

wear of the inner and outer rails is the most intense at the gauge corner with the maximum value reaching 1.81mm. The wear of the guard rail is the lightest and the maximum value is only 0.3mm. With the change of wheel-rail friction coefficient from 0.2 to 0.4, the average wear rate of inner rail head is 54.02% and the inner gauge corner is 41.72% and the inner guard rail is 187.5%. The average wear rate of outer rail head is 83.56% and the outer gauge corner is 49.34% and the outer guard rail is 100%.

Figure 14 is the wheel profile change after tram passed 500 km through the curved track repeatedly shown in Fig. 8 under three wheel-rail friction coefficients: 0.2, 0.3 and 0.4. Figure 15 is the inner and outer wheel wear after tram passed 500 km under three friction coefficients. Table 3 is the maximum wheel wear after tram passed 500 km under three friction coefficients.

(a) Inner rail

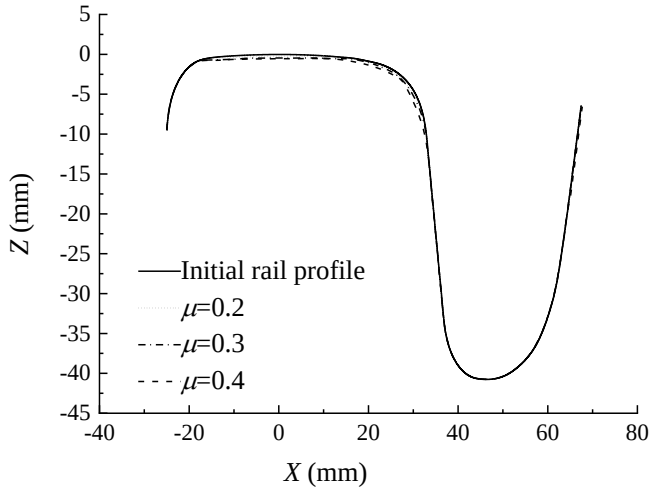

(b) Enlarged diagram of inner rail

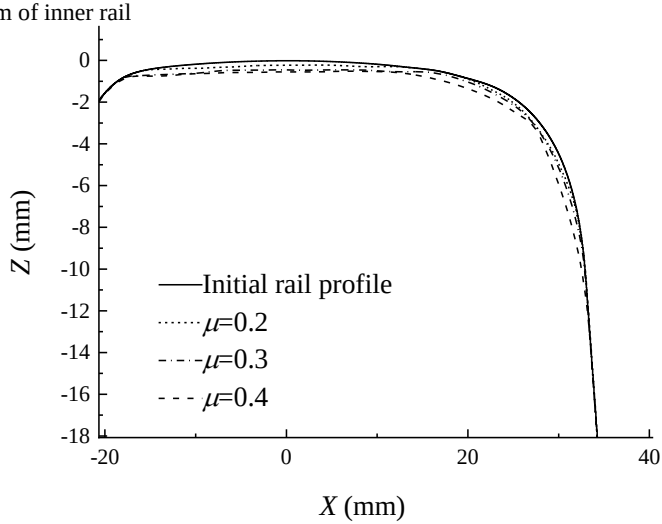

Fig.12. (a)-(b). Diagram of rail profile change after tram passed 68 000 times under three friction coefficients

(c) Outer rail

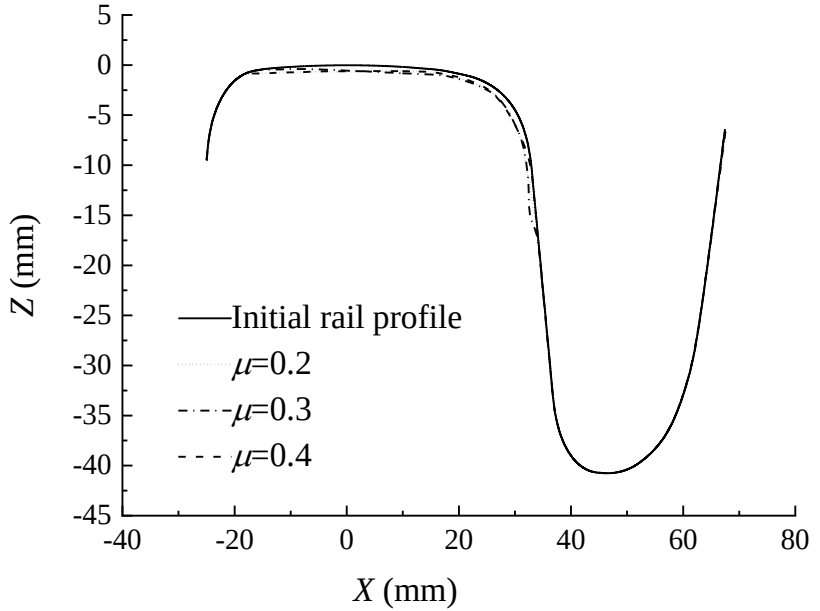

(d) Enlarged diagram of outer rail

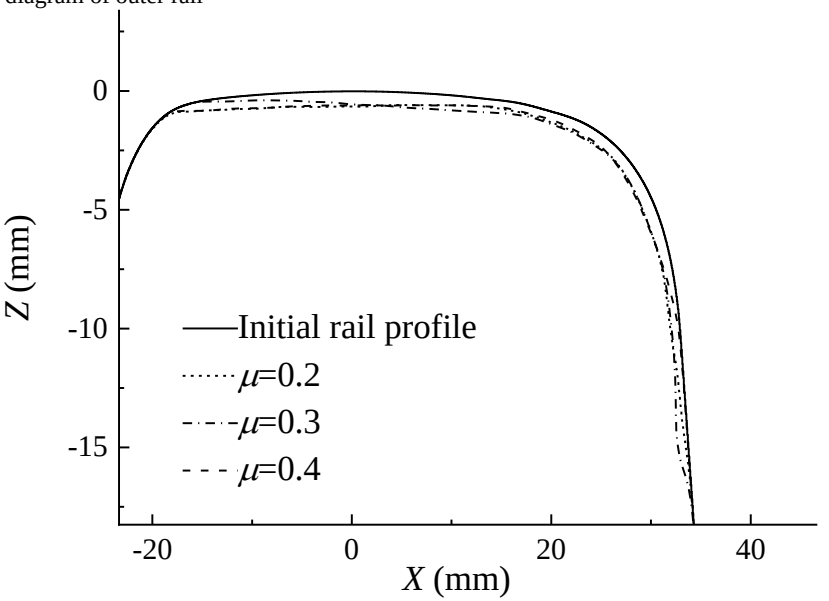

Fig.12. (c)-(d). Diagram of rail profile change after tram passed 68 000 times under three friction coefficients

(a) Inner rail

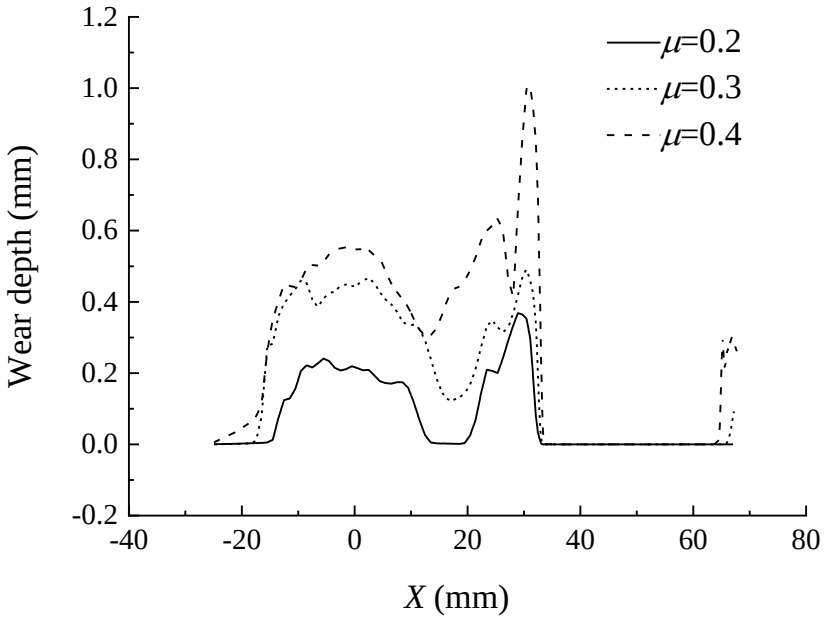

(b) Outer rail

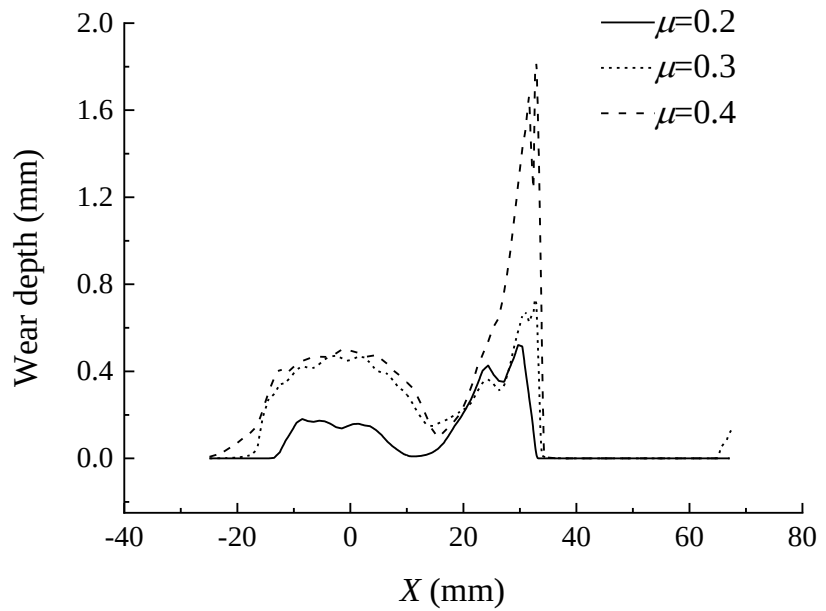

Fig.13. Diagram of inner and outer rail wear after tram passed 68 000 times under three friction coefficients

Table. 2. Maximum rail wear after tram passed 68 000 times under three friction coefficients

Friction coefficient	**Inner rail/mm**					
0.2	Rail head	0.24	Gauge corner	0.37	Guard rail	0
0.3	Rail head	0.46	Gauge corner	0.49	Guard rail	0.08
0.4	Rail head	0.55	Gauge corner	1.00	Guard rail	0.30
Friction coefficient	**Outer rail/mm**					
0.2	Rail head	0.18	Gauge corner	0.52	Guard rail	0
0.3	Rail head	0.47	Gauge corner	0.72	Guard rail	0.13
0.4	Rail head	0.50	Gauge corner	1.81	Guard rail	0

(a) Inner wheel of wheelset one

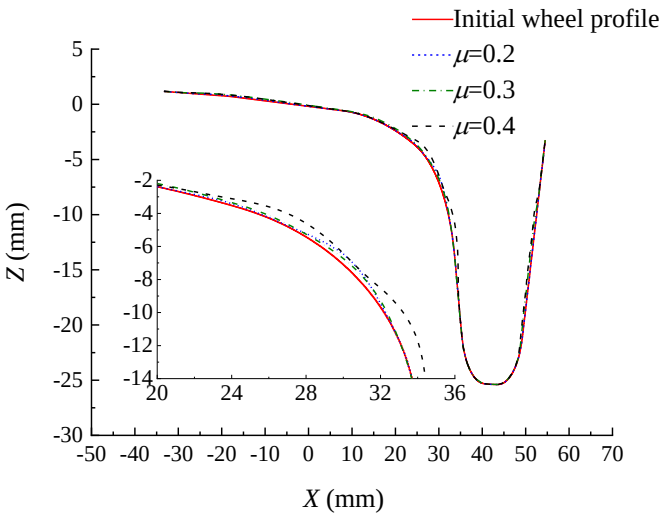

(b) Outer wheel of wheelset one

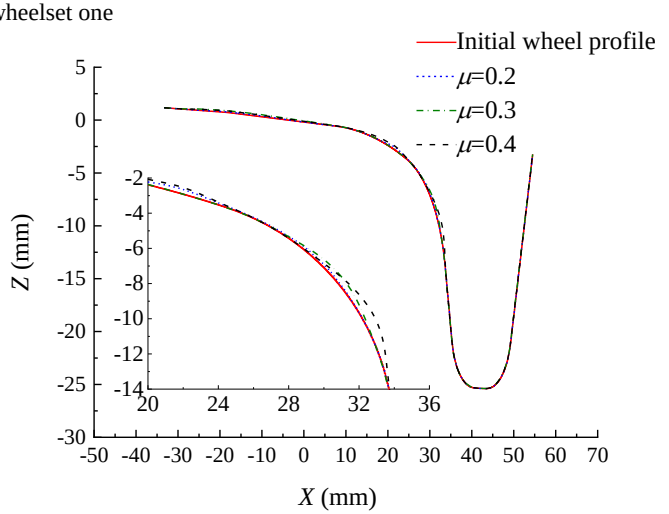

Fig.14. (a)-(b). Diagram of wheel profile change after tram passed 500 km under three friction coefficients

(c) Inner wheel of wheelset three

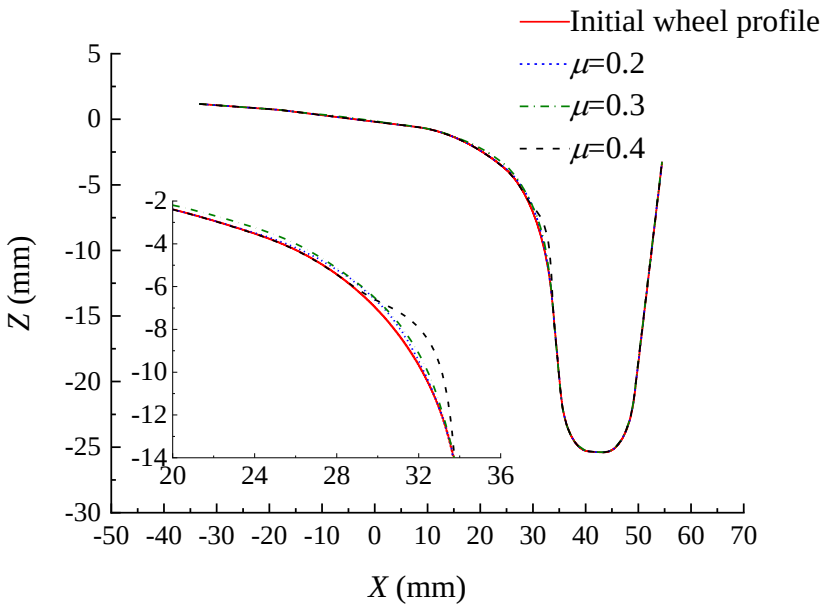

(d) Outer wheel of wheelset three

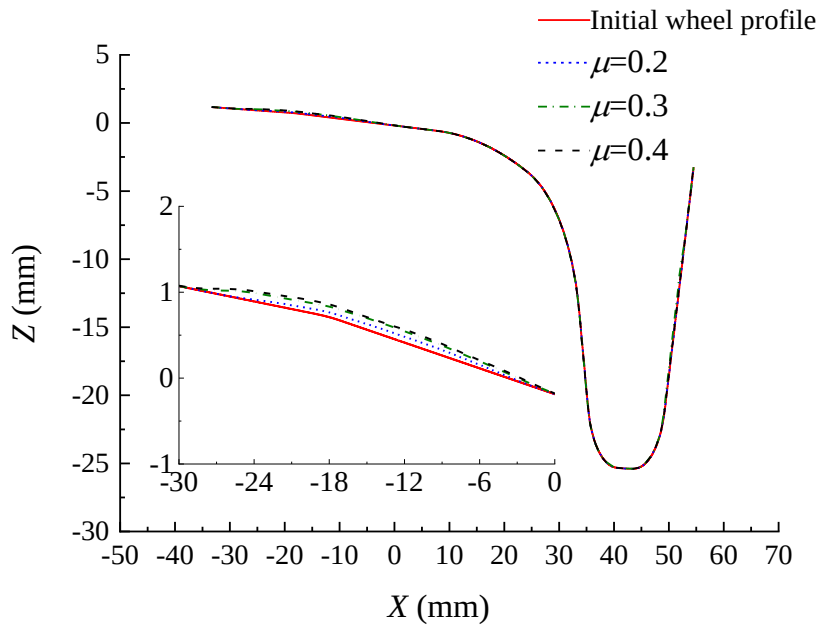

Fig.14. (c)-(d). Diagram of wheel profile change after tram passed 500 km under three friction coefficients

(a) Inner wheel of wheelset one

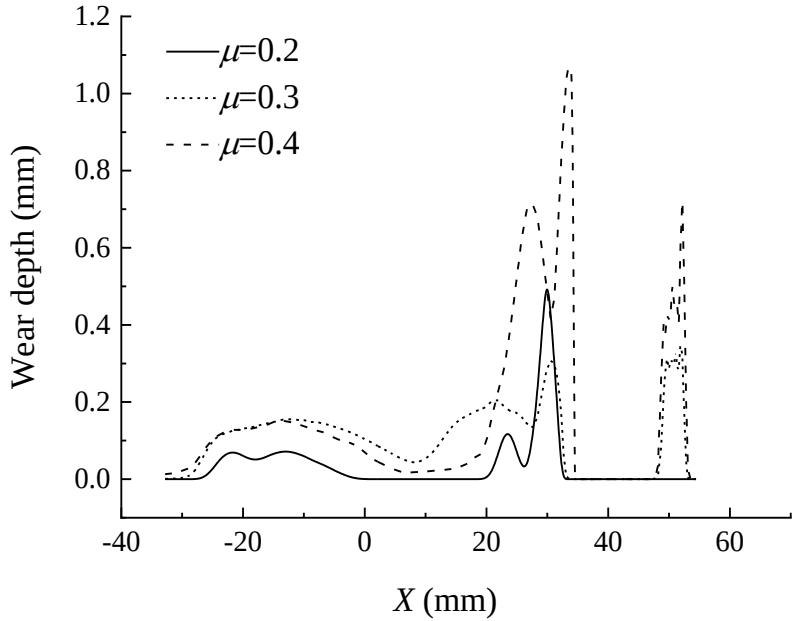

(b) Outer wheel of wheelset one

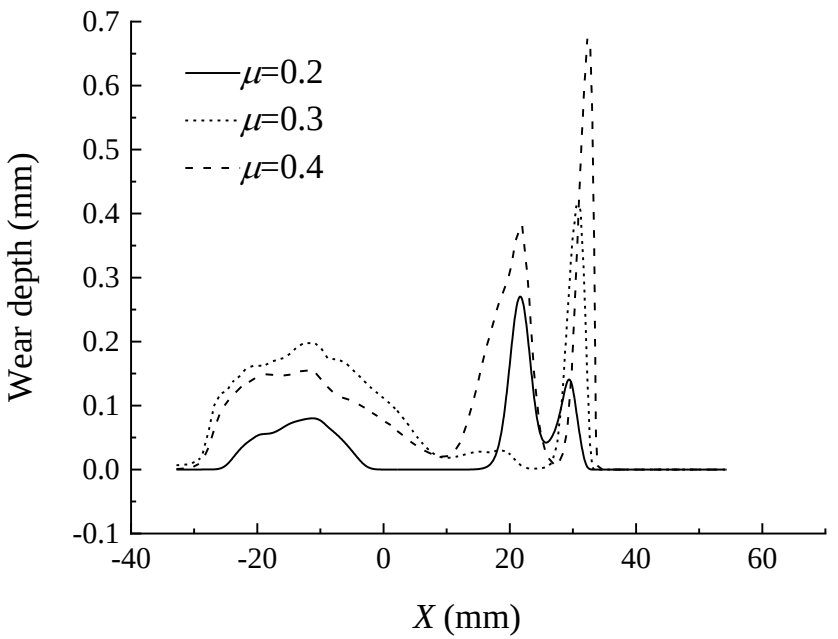

Fig.15. (a)-(b). Diagram of inner and outer wheel wear after tram passed 500 km under three friction coefficients

(c) Inner wheel of wheelset three

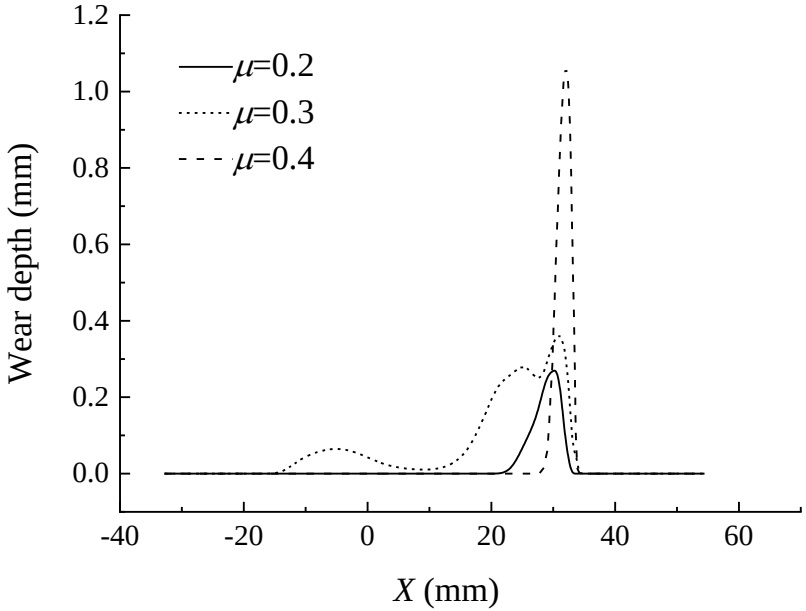

(d) Outer wheel of wheelset three

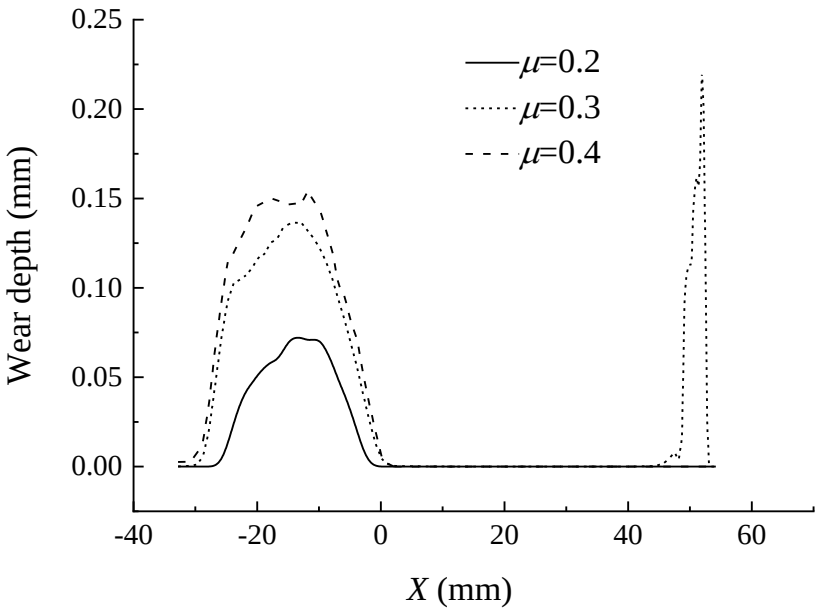

Fig.15. (a)-(b). Diagram of inner and outer wheel wear after tram passed 500 km under three friction coefficients

Table. 3. Maximum wheel wear after tram passed 500 km under three friction coefficients

Friction coefficient	**Inner wheel of wheelset one/mm**					
0.2	Tread	0.08	Wheel flange	0.50	Wheel back	0.15
0.3	Tread	0.16	Wheel flange	0.31	Wheel back	0.30
0.4	Tread	0.18	Wheel flange	1.07	Wheel back	0.45
Friction coefficient	**Outer wheel of wheelset one/mm**					
0.2	Tread	0.09	Wheel flange	0.14	Wheel back	0
0.3	Tread	0.20	Wheel flange	0.41	Wheel back	0
0.4	Tread	0.18	Wheel flange	0.67	Wheel back	0
Friction coefficient	**Inner wheel of wheelset three/mm**					
0.2	Tread	0	Wheel flange	0.27	Wheel back	0
0.3	Tread	0.05	Wheel flange	0.36	Wheel back	0
0.4	Tread	0	Wheel flange	1.06	Wheel back	0
Friction coefficient	**Outer wheel of wheelset three/mm**					
0.2	Tread	0.07	Wheel flange	0	Wheel back	0
0.3	Tread	0.13	Wheel flange	0	Wheel back	0.22
0.4	Tread	0.15	Wheel flange	0	Wheel back	0

It can be seen from Figure 14, Figure 15 and Table 3 that there is an increasing trend of the inner and outer wheel wear of wheelset one but there is no obvious change of the inner and outer wheel wear of wheelset three. Comparing the wear of wheelsets one and three, it can be seen that the wear of wheelset one is more intense than that of wheelset three. The total wear of wheelset one is 112% more than that of wheelset three. Comparing the inner and outer wheel wear, it can be seen that the inner wheel wear is more intense than that of the outer wheel. The total wear of the inner wheel is 119% more than that of the outer wheel.

With the change of wheel-rail friction coefficient from 0.2 to 0.4, the average wear rate of inner wheel tread of wheelset one is 55.56% and the wheel flange is 16.51% and the wheel back is 66.67%.

With the change of wheel-rail friction coefficient, the average wear rate of outer wheel tread of wheelset one is 55.56% and the wheel flange is 115.83% and the wheel back is 0%.

With the change of wheel-rail friction coefficient, the average wear rate of inner wheel tread of wheelset three is 100% and the wheel flange is 49.69% and the wheel back is 0%.

With the change of wheel-rail friction coefficient, the average wear rate of outer wheel tread of wheelset three is 49.52% and the wheel flange is 0% and the wheel back is 100%.

4. Conclusions

To improve the life of tram wheel and rail and reduce the frequency of wheel-rail maintenance during operation, the wear of rails and wheels of modern trams in the front and rear transition curves and circular curves was explored on the small curved track with a radius of 50 m by establishing the wheel-rail wear prediction model. The following conclusions can be drawn:

(1) On the small radius curve, the rail wear on the circular curve and the rear transition curve is much larger than that of the front transition curve, and the wear on the rear transition curve is the most intense. The total rail wear on the rear transition is 119% of the total wear on the circular curve and 344% of the total wear on the front transition curve.

(2) Compared with the front transition curve, the wheel wear on the circular curve and the rear transition curve is more intense. The total wheel wear on the circular curve is 120% of the total wear on the rear transition curve and 308 % of the total wear on the front transition curve.

(3) The wear of inner and outer rail increases with the increase of wheel-rail friction coefficient. The wear of the inner and outer rails is the most intense at the gauge corner position with the maximum value reaching 1.81 mm. The wear of the guard rail is the lightest and the maximum value is only 0.3 mm.

(4) There is an increasing trend of the inner and outer wheel wear of wheelset one with the increase of wheel-rail friction coefficient but there is no obvious change of the inner and outer wheel wear of wheelset three. The wear of wheelset one is more intense than that of wheelset three and the inner wheel wear is more intense than that of the outer wheel.

Acknowledgments
This research was supported by the National Natural Science Foundation of China (No.52178436), and sponsored by Shanghai Collaborative Innovation Research Center for Multi-network & Multi-modal Rail Transit.

References

1. Zeng, Z.P., Huang, X.D., Wang, J.D., Liu, F.S., Wang, W.D., & Shuaibu, A.A. (2021). Wheel-rail stochastic dynamics and rail wear analysis of small radius curved sections of a tram line based on generalized probability density evolution. *Proceedings of the Institution of Mechanical Engineers Part F-Journal of Rail and Rapid Transit, 235*(5), 543-558. https://doi.org/10.1177/0954409720947533
2. Suda, Y., & Michitsuji, Y. (2023). Improved curving performance using unconventional wheelset guidance design and wheel-rail interface-present and future solutions. *Vehicle System Dynamics*, 2199937. https://doi.org/10.1080/00423114.2023.2199937
3. Chi, M.R., Zhang, W.H., Zeng, J., Dai, H.Y., & Wu, P.B. (2008). New flexible coupled radial bogie with independently rotating wheels. *Chinese Journal of Mechanical Engineering*, *44*(3), 9-15. https://doi.org/10.3901/JME.2008.03.009
4. Zhu, A.H., Yang, S., Li, Q., Yang, J.W., Fu, C.Z., Zhang, J., & Yao, D.C. (2019). Research on prediction of metro wheel wear based on integrated data-model-driven approach. *IEEE Access*, *7*, 178153-178166. https://doi.org/10.1109/ACCESS.2019.2950391
5. Pradhan, S., Samantaray, A.K., & Bhattacharyya, R. (2019). Multistep wear evolution simulation method for the prediction of rail wheel wear and vehicle dynamic performance. *Simulation*, *95*(5), 441-459. https://doi.org/10.1177/0037549718785023
6. Wang, M.Q., Jia, S.X., Chen, E.L., Yang, S.P., Liu, P.F., & Qi, Z. (2022a). Research and application of neural network for tread wear prediction and optimization. *Mechanical Systems and Signal Processing*, *162*, 108070. https://doi.org/10.1016/j.ymssp.2021.108070
7. Li, Y.Y., Ren, Z.R., Enblom, R., Stichel, S., & Li, G.D. (2020). Wheel wear prediction on a high-speed train in China. *Vehicle System Dynamics*, *58*(12), 1839-1858. https://doi.org/10.1080/00423114.2019.1650941
8. Chudzikiewicz, A., & Korzeb, J. (2018). Simulation study of wheels wear in low-floor tram with independently rotating wheels. *Arch Appl Mech*, *88*, 175-192. https://doi.org/10.1007/s00419-017-1301-6
9. Wang, L., Xu, H., Yuan, H., Zhao, W.J., & Chen, X.A. (2015). Optimizing the re-profiling strategy of metro wheels based on a data-driven wear model. *European Journal of Operational Research*, *242*, 975-986. https://doi.org/10.1016/j.ejor.2014.10.033
10. Zeng, Y.C., Song, D.L., Zhang, W.H., Zhou, B., Xie, M.Y., & Tang, X. (2020). A new physics-based data-driven guideline for wear modelling and prediction of train wheels. *Wear*, *456-457*, 203355. https://doi.org/10.1016/j.wear.2020.203355
11. Wang, S.W., Guo, H., Zhang, S.Y., Barton, D., & Brooks, P. (2022b). Analysis and prediction of double-carriage train wheel wear based on SIMPACK and neural networks. *Advances in Mechanical Engineering*, *14*(3), 1-12. https://doi.org/10.1177/16878132221078491
12. Shebani, A., & Iwnicki, S. (2018). Prediction of wheel and rail wear under different contact conditions using artificial neural networks. *Wear*, *406-407*, 173-184. https://doi.org/10.1016/j.wear.2018.01.007
13. Wang, S.W., Yan, H., & Liu, C.X. (2018). Analysis and prediction of high-speed train wheel wear based on SIMPACK and backpropagation neural networks. *Expert Systems*, *38*, e12417. https://doi.org/10.1111/exsy.12417
14. Cai, H., Wang, Y.L., Song, C.W., Wang, T.T., & Shen, Y. (2022). Prediction of surface subsidence based on PSO-BP neural network. *Journal of Physics: Conference Series*, *2400*, 012046. https://doi.org/10.1088/1742-6596/2400/1/012046

15. Su, K.X., Zhang, J.W., Zhang, J.W., Yan, T., & Mei, G.M. (2023). Optimisation of current collection quality of high-speed pantograph-catenary system using the combination of artificial neural network and genetic algorithm. *Vehicle System Dynamics*, *61*(1), 260-285. https://doi.org/10.1080/00423114.2022.2045029
16. Zhao, W., Wang, C.Y., Zhang, J., & Du, L.M. (2011). Research on matching of railway wheel and rail profiles. *Journal of the China Railway Society*, *33*(02), 34-37. https://doi.org/10.3969/j.issn.1001-8360.2011.02.006
17. Liu, S.Y., Lei, Z.Y., & Yao, X. (2024). Rail wear characteristics of small curve section in modern Tram. *Traffic & Transportation*, *40*(02), 57-61. https://doi.org/1671-3400(2024)02-0057-05
18. Łuczak, B., Firlik, B., Stas´kiewicz, T., & Sumelka, W. (2020). Numerical algorithm for predicting wheel flange wear in trams - Validation in a curved track. *Proc IMechE Part F: J Rail and Rapid Transit*, *234*(10), 1156-1169. https://doi.org/10.1177/0954409719882807
19. Zhong, X.B., Tao, G.A., Luo, Y.Y., & Yi, X.L. (2016). Optimization method for independently rotating wheel profiles. *Journal of Sichuan University of Science & Engineering (Natural Science Edition)*, *29*(03), 33-38. https://doi.org/10.11863/j.suse.2016.03.08
20. Yang, X.W., Liu, S.T., & Hu, Y.H. (2022). Optimal design of profile of groove shaped rail of modern trams. *Journal of Tongji University (Natural Science)*, *50*(06), 891-898. https://doi.org/10.11908/j.issn.0253-374x.21392
21. Wojciechowski, Ł., Gapinski, B., Firlik, B., & Mathia, T.G. (2020). Characteristics of tram wheel wear: Focus on mechanism identification and surface topography. *Tribology International*, *150*, 106365. https://doi.org/10.1016/j.triboint.2020.106365
22. Zehetbauer, F., Edelmann, J., & Plöchl, M. (2024). Influences of tram characteristics on wheel polygonal wear evolution. *Engineering Failure Analysis*, *157*, 107528. https://doi.org/10.1016/j.engfailanal.2023.107528
23. Yang, X.W., Liu, X.S., Shen, J.G., & Meng, W. (2019). Effect of rail cant on groove-shaped rail wear in modern tram line. *Journal of Tongji University (Natural Science)*, *47*(04), 528-534. https://doi.org/10.11908/j.issn.0253-374x.2019.04.011
24. Ding, J.J., Yang, Y., Li, F., Huang, Y.H., & Jiang, K. (2017). Research on wheel wear and optimization of low-floor trams based on groove track. *Journal of the China Railway Society*, *39*(7), 54. https://doi.org/10.3969/j.issn.1001-8360.2017.07.008